

RESEARCH

Open Access



# Experimental mechanical characterisation, regression-based modelling and life cycle assessment of surface-modified jute fibre reinforced recycled PET composites

G. Anbuhezhiyan<sup>1</sup>, S. Saravana Mahesan<sup>1</sup>, Senthil Babu<sup>2</sup>, S. Thirumalai Kumaran<sup>3</sup>, Oisik Das<sup>4\*</sup> and Vigneshwaran Shanmugam<sup>4\*</sup>

\*Correspondence:

Oisik Das  
oisik.das@ltu.se  
Vigneshwaran Shanmugam  
s.vigneshwaren@gmail.com  
<sup>1</sup>Department of Mechanical Engineering, Vel Tech Rangarajan Dr. Sagunthala R&D Institute of Science and Technology, Avadi, Chennai 600062, Tamil Nadu, India

<sup>2</sup>Department of Mechanical Engineering, SRM Institute of Science and Technology, Ramapuram Campus, Chennai, Tamil Nadu, India

<sup>3</sup>Department of Mechanical Engineering, PSG Institute of Technology and Applied Research, Coimbatore 641062, Tamil Nadu, India

<sup>4</sup>Fire Technology, Department of Civil, Environmental and Natural Resources Engineering, Luleå University of Technology, Luleå 97187, Sweden

## Abstract

The accumulation of post-consumer polyethylene terephthalate (PET) waste necessitates value-added recycling strategies that restore mechanical performance while maintaining environmental sustainability. In this study, recycled PET (rPET) was reinforced with 20 wt% short jute fibres subjected to untreated (UT), NaOH-treated (NT), and silane-treated (ST) surface modifications. Composites were fabricated by injection moulding and characterised using X-ray diffraction and FTIR to confirm removal of amorphous constituents and formation of interfacial siloxane linkages. Surface treatment improved consolidation, with experimental density increasing from 1.22 to 1.24 g/cm<sup>3</sup> and porosity decreasing from 3.9% to 2.4%. Correspondingly, tensile strength increased from 38.78 to 48.29 MPa, flexural strength from 50.30 to 68.84 MPa, short-beam shear strength from 11.74 to 14.66 MPa, and hardness from 77 to 81 Shore D. One-way ANOVA confirmed statistically significant improvements ( $p < 0.05$ ). Porosity-based linear regression modelling demonstrated strong structure–property relationships ( $R^2 = 0.631–0.916$ ), with cross-validated  $R^2$  values of 0.391–0.861, indicating moderate predictive robustness within the investigated domain. A cradle-to-gate life cycle assessment revealed low carbon footprints (2.49–2.51 kg CO<sub>2</sub>-eq kg<sup>-1</sup>), with fibre surface modification introducing only marginal environmental penalties. The results demonstrate that surface-engineered jute fibres effectively enhance the mechanical integrity of recycled PET while maintaining favourable sustainability performance.

**Keywords** Recycled PET composites, Jute fibre, Surface modification, Alkali and silane treatment, Mechanical properties, Life cycle assessment (LCA)

## 1 Introduction

In 2025, global plastics production is projected to reach nearly 500 million tonnes, generating more than 400 million tonnes of waste, releasing almost two gigatons of greenhouse gases and leaking over 24 million tonnes of plastics including micro- and



© The Author(s) 2026. **Open Access** This article is licensed under a Creative Commons Attribution 4.0 International License, which permits use, sharing, adaptation, distribution and reproduction in any medium or format, as long as you give appropriate credit to the original author(s) and the source, provide a link to the Creative Commons licence, and indicate if changes were made. The images or other third party material in this article are included in the article's Creative Commons licence, unless indicated otherwise in a credit line to the material. If material is not included in the article's Creative Commons licence and your intended use is not permitted by statutory regulation or exceeds the permitted use, you will need to obtain permission directly from the copyright holder. To view a copy of this licence, visit <http://creativecommons.org/licenses/by/4.0/>.

nanoplastics into terrestrial and aquatic ecosystems [1]. A significant proportion of this waste is derived from disposable beverage containers made from polyethylene terephthalate (PET). According to the United Nations Environment Programme (UNEP, 2024), PET-based packaging contributes approximately 12–14% of global thermoplastic waste, with water-bottle disposal alone exceeding 25 million tonnes year<sup>-1</sup> [2]. Mechanical recycling of these bottles into recycled PET (rPET) offers a promising circular-material solution that decreases dependence on virgin petrochemical feedstock [3]. However, rPET generated from bottle flakes typically undergoes polymer-chain scission and loss of intrinsic viscosity, resulting in up to reductions in mechanical strength and performance compared with virgin PET grades [4]. These limitations restrict its structural utilisation, particularly in applications where stiffness, load-bearing capacity, and reliability are critical.

Reinforcing recycled PET with renewable natural fibres presents a sustainable approach to restoring its mechanical integrity while simultaneously reducing carbon footprint and material cost. Natural-fibre reinforcement aligns with global sustainability initiatives, including UN Sustainable Development Goal 12 on Responsible Consumption and Production, by enabling circular resource flows and lowering environmental impact [5]. Natural fibres often show limited interfacial adhesion with polyester matrices such as PET, despite their moderate polarity, due to differences in surface chemistry and the hydroxyl-rich nature of lignocellulosic fibres. This mismatch in surface functionality can lead to poor wettability, increased porosity, weak interfacial bonding, and premature interfacial failure in untreated composites [6]. While extensive work has investigated natural-fibre composites based on virgin polymers, comparatively few studies have optimised fibre–matrix interactions in recycled PET systems. Furthermore, most available research emphasises macroscopic mechanical testing without integrating predictive modelling to quantitatively relate microstructural attributes such as experimental density ( $\rho_c$ ) and porosity to mechanical responses. Closing this knowledge gap is essential for designing next-generation sustainable composites from post-consumer plastics.

Natural fibres such as jute, flax, sisal, kenaf, and hemp offer attractive characteristics including low density (1.3–1.5 g/cm<sup>3</sup>), favourable specific strength, biodegradability, and carbon neutrality [7, 8]. Among these, jute fibre is particularly promising due to its global availability (3.4 million tonnes year<sup>-1</sup>), tensile strength of 400–800 MPa, modulus of 10–30 GPa, and low production cost [9–11]. However, raw jute contains significant amounts of lignin (10–12%), hemicellulose (18–20%), and waxes (1–2%), which form a weak boundary layer that impedes adhesion with polymer matrices [12, 13]. Chemical surface treatments are therefore essential: alkaline (NaOH) treatment removes amorphous components, increases surface roughness, and enhances fibre wettability by exposing cellulose hydroxyl groups [14]. Silane coupling agents such as  $\gamma$ -aminopropyltriethoxysilane (APTES) further introduce Si–O–C and Si–O–Si linkages that chemically anchor fibres to the polymer matrix [15, 16]. Previous studies have shown substantial improvements after such modifications: Hai et al. [17] reported up to ca. 40% increases in tensile strength for treated jute polypropylene (PP) composites, while Ravindran et al. [18] observed ca. 19% higher tensile strength in silane-treated jute/vinylester composite. However, applications of these treatments to rPET—particularly bottle-derived rPET—remain limited.

Parallel to advances in fibre surface modification, statistical modelling approaches are increasingly employed to quantify structure–property relationships in composite materials [19, 20]. Linear techniques such as multiple linear regression (MLR) and regression-based response modelling provide transparent and physically interpretable correlations between microstructural parameters and mechanical performance [21, 22]. Unlike purely empirical comparisons, regression analysis enables identification of dominant governing variables and quantification of their influence within defined experimental domains. Several studies have successfully applied regression-based approaches to relate fibre content, void fraction, and processing parameters to tensile and flexural responses in polymer composites [23, 24]. However, most investigations of natural-fibre reinforced recycled polymers focus primarily on reporting mechanical properties without explicitly linking them to measurable structural indicators such as experimental density or porosity. The quantitative relationship between fibre surface chemistry, void reduction, and resulting mechanical performance remains insufficiently explored, particularly for bottle-derived recycled PET systems. Establishing clear porosity–property correlations is essential for developing preliminary design guidelines and for enabling data-driven optimisation of sustainable composite formulations. Addressing this gap contributes to improved predictability, material efficiency, and circular-economy implementation in recycled thermoplastic composites.

Life-cycle assessment (LCA) studies indicate that natural-fibre reinforcement of polymers can significantly reduce greenhouse-gas emissions and embodied energy compared with synthetic-fibre or virgin-polymer systems [25]. For example, Korol *et al.* [26] showed that incorporating 30 wt% jute fibre into a PP matrix reduced the carbon footprint by about 18% compared with neat PP, while also giving lower carbon and ecological footprints than glass-fibre-reinforced PP in an EUR-pallet case study. Recent LCA work on textile–natural fibre hybrid composites by Arya *et al.* [27] further showed that flax–recycled polyester laminates exhibited the lowest environmental impact across 18 midpoint impact categories, outperforming pure flax laminates and flax–polyamide systems. Additionally, diverting agricultural residues such as jute prevents decomposition-related methane release, providing further greenhouse-gas mitigation. Collectively, these LCA findings highlight the significant decarbonisation potential of natural-fibre composites, especially when combined with recycled polymer or textile streams within circular-economy frameworks.

The present work addresses these gaps by developing rPET–jute fibre composites derived from post-consumer water-bottle waste through injection moulding. Untreated, NaOH-treated, and silane-treated jute fibres were incorporated to systematically investigate the influence of surface modification on microstructural characteristics, including density and porosity, as well as tensile, flexural, short-beam shear, and hardness responses. Structural and chemical changes in the fibres were characterised using X-ray diffraction (XRD) and Fourier-transform infrared spectroscopy (FTIR). Quantitative structure–property relationships were established using porosity-based linear regression modelling to evaluate the influence of consolidation quality on mechanical performance. This integrated experimental and statistical approach aims to provide a transparent framework for correlating fibre surface chemistry, void content, and mechanical behaviour in recycled PET composites, thereby supporting the development of mechanically improved and resource-efficient thermoplastic materials.

## 2 Materials and methods

### 2.1 Materials

rPET was recovered from post-consumer PET water and beverage bottles collected from a local recycling unit in Chennai, India. The bottles were thoroughly cleaned using a mild detergent solution, rinsed with deionised water, and dried in an oven at 60 °C for 24 h to remove residual moisture prior to shredding. The dried bottles were then shredded into flakes and melt-processed using a single-screw extruder at 250 °C to obtain rPET pellets. To minimise hydrolytic degradation during subsequent melt processing, the rPET pellets were dried again at 60 °C for 24 h in an oven prior to composite compounding. Long jute fibres (average diameter  $\approx$  150  $\mu\text{m}$ , true density = 1.45  $\text{g}/\text{cm}^3$ ) were procured from Tokyo Fibres, Coimbatore, India. Prior to use, the long fibres were manually cut into short fibres of 4–5 mm length for composite manufacturing. Analytical-grade sodium hydroxide (NaOH, 98%) and  $\gamma$ -aminopropyltriethoxysilane (APTES, 99%) were employed for fibre surface modification.

### 2.2 Fibre treatment

The raw jute fibres were first washed with distilled water to remove surface impurities and oven-dried at 60 °C for 4 h. Alkali treatment was carried out by immersing the fibres in a 5 wt% NaOH solution at room temperature for 2 h. The treated fibres were then thoroughly rinsed with distilled water until the pH of the rinse water was neutral and dried again at 60 °C for 6 h. For silane treatment, the alkali-treated fibres were soaked in a 2 wt% silane solution prepared in a 95:5 ethanol–water mixture (pH 4.5 adjusted using acetic acid) for 1 h at room temperature. The fibres were subsequently filtered, oven-dried at 60 °C for 8 h, and stored in sealed polyethylene bags prior to compounding.

### 2.3 Fibre characterisation - XRD and FTIR

The crystalline structure of the fibres was analysed using XRD on a Cu K $\alpha$  radiation source ( $\lambda = 1.5406 \text{ \AA}$ ) operating at 40 kV and 30 mA. Scans were recorded in the  $2\theta$  range of 10–40° at a step size of 0.02°. The crystallinity index (CI) was calculated using Segal's empirical relation:

$$\text{CI}(\%) = \frac{I_{200} - I_{\text{am}}}{I_{200}} \times 100 \quad (1)$$

where  $I_{200}$  is the maximum intensity of the (200) diffraction peak at around 22°  $2\theta$ , and  $I_{\text{am}}$  is the minimum peak height between 18° and 19°  $2\theta$  corresponding to the amorphous region. The crystallite size ( $D$ ) of cellulose was estimated using the Scherrer equation:

$$D = \frac{K\lambda}{\beta \cos\theta} \quad (2)$$

where  $K = 0.89$  is the shape factor,  $\beta$  is the full width at half maximum (FWHM) of the (200) peak (in radians), and  $\theta$  is the Bragg angle.

### 2.4 Composite fabrication

Composites were fabricated by the injection moulding method using 20 wt% chopped jute fibre and 80 wt% rPET as the matrix material. The rPET pellets and short jute fibres

were accurately weighed and premixed in a high-speed mechanical blender for 10 min to achieve uniform fibre distribution. The blended mixture was then melt-compounded using a co-rotating twin-screw extruder. The barrel temperatures were maintained at 230 °C in the feed zone, 235 °C in the middle zone, and 240 °C at the die zone to ensure complete melting of the rPET and uniform fibre dispersion while avoiding thermal degradation. The screw speed was kept constant at 80 rpm, and the average residence time was approximately 4 min. The extruded composite strands were cooled in a circulating water bath, pelletised, and dried at 60 °C for 6 h in an oven prior to injection moulding. This final drying step was performed immediately before moulding to minimise moisture-induced hydrolysis during melt processing.

Injection moulding was carried out to produce standard test specimens. The barrel temperature profile was set to 250 °C, with a nozzle temperature of 240 °C. The injection pressure was maintained at 70 MPa, and the mould temperature was controlled at 40 °C to ensure complete filling and minimise shrinkage. Three composites were fabricated under identical processing conditions: neat, untreated fibre-reinforced rPET (UT), NaOH-treated fibre-reinforced rPET (NT), and silane-treated fibre-reinforced rPET (ST). All the moulded specimens were conditioned at  $25 \pm 2$  °C and  $50 \pm 5\%$  relative humidity for 48 h before mechanical testing to ensure dimensional stability and uniform moisture content. Figure 1 shows the process flow of rPET–jute composite fabrication and characterisation.

## 2.5 Density and porosity determination

Experimental density ( $\rho_e$ ) was measured using the Archimedes principle (ASTM D792) with distilled water as the immersion medium. The theoretical density ( $\rho_t$ ) of the composite was calculated using the rule of mixtures:

$$\rho_t = W_f \rho_f + W_m \rho_m \quad (3)$$

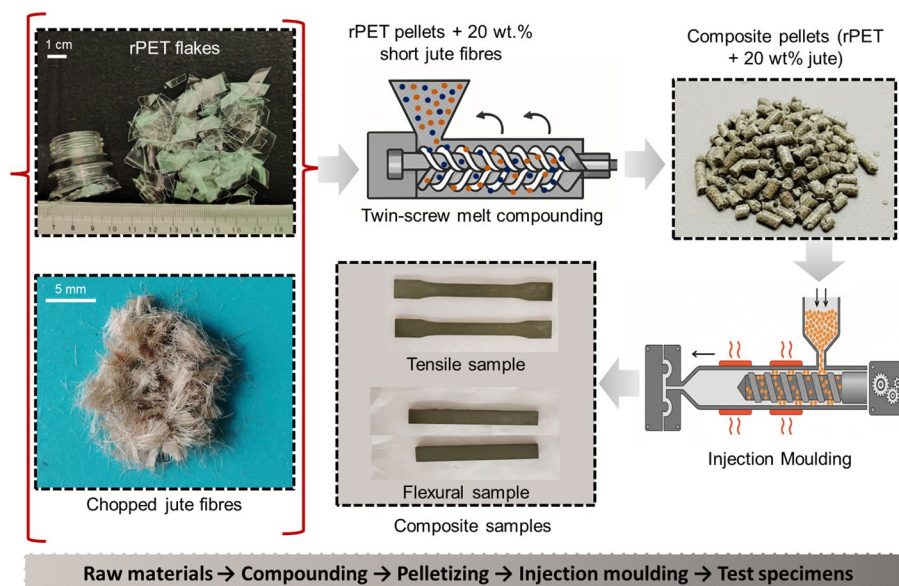


**Fig. 1** Process flow of rPET–jute composite fabrication and characterisation

where  $W_f = 0.20$ ,  $W_m = 0.80$ ,  $\rho_f = 1.45\text{gcm}^{-3}$ , and  $\rho_m = 1.23\text{gcm}^{-3}$ , yielding  $\rho_t = 1.27\text{gcm}^{-3}$ . The porosity (%) of each composite was determined from the difference between theoretical and experimental densities using

$$\text{Porosity (\%)} = \frac{(\rho_t - \rho_e)}{\rho_t} \times 100. \quad (4)$$

## 2.6 Tensile test

The tensile behaviour of the rPET/jute fibre composites was evaluated according to ASTM D638 using dog-bone specimens. The samples had dimensions of 165 mm  $\times$  13 mm  $\times$  3 mm, with a gauge length of 50 mm in the reduced section. Tests were performed on a TEC-SOL universal testing machine (50 kN load cell) at room temperature ( $25 \pm 2$  °C). A constant crosshead speed of 2 mm  $\text{min}^{-1}$  was used. For each material condition (Neat, UT, NT, and ST), three specimens were tested, and the mean and standard deviation were reported. This sample size follows the minimum requirement of relevant ASTM standards for comparative mechanical testing of thermoplastic composites. All specimens were produced under identical extrusion and injection-moulding conditions to minimise variability. The results are therefore used to compare relative performance trends between different fibre treatments rather than to establish absolute material properties.

## 2.7 Flexural test

Flexural properties were measured by three-point bending following ASTM D790. Rectangular bars of approximately 100 mm  $\times$  12.7 mm  $\times$  3 mm were used. Each specimen was tested using a three-point bending fixture with a support span-to-depth ratio of 16:1. The crosshead speed was set to 1.5 mm  $\text{min}^{-1}$ . Flexural strength ( $\sigma$ ) and flexural modulus ( $E_f$ ) were evaluated from the load–deflection data using standard beam-bending relations:

$$\sigma_f = \frac{3FL}{2bd^2} \quad (5)$$

$$E_f = \frac{L^3m}{4bd^3} \quad (6)$$

where  $F$  is the applied load at the outer surface at a given deflection,  $L$  is the support span,  $b$  is the specimen width,  $d$  is the specimen thickness, and  $m$  is the slope of the initial.

## 2.8 Short-Beam Shear Strength (SBSS)

Short-beam shear strength was determined using a short-beam test in accordance with ASTM D2344. Specimens with nominal dimensions of 20 mm  $\times$  6 mm  $\times$  3 mm were used. Each specimen was loaded over a short span of 12 mm, corresponding to a span-to-thickness ratio of approximately 4:1. The crosshead speed was maintained at 1 mm  $\text{min}^{-1}$ .

The short-beam shear strength ( $\tau$ ) was calculated using:

$$\tau = \frac{0.75F_{\max}}{bh} \quad (7)$$

where  $F_{\max}$  is the maximum load prior to failure,  $b$  is the specimen width, and  $h$  is the specimen thickness. The measured values are used as a comparative indicator of shear-dominated fibre–matrix interfacial resistance, rather than true interlaminar shear strength as defined for laminated composites.

### 2.9 Hardness test

Surface hardness was evaluated using a Shore D durometer in accordance with ASTM D2240. Prior to testing, the composites surface was cleaned and the indenter was applied perpendicular to the surface under standard force, and the hardness value was recorded after a 15 s dwell time to allow the indenter to reach equilibrium penetration. For each formulation, three hardness measurements were taken at spatially separated locations to avoid local damage effects and anisotropy from fibre orientation. The reported hardness for each composite was calculated as the arithmetic mean of these readings.

### 2.10 Statistical analysis (ANOVA)

A one-way analysis of variance (ANOVA) was performed to assess the statistical significance of variations in the mechanical properties among the four composite groups Neat, UT, NT, and ST. The analysis was carried out at a 95% confidence level ( $\alpha = 0.05$ ). Prior to ANOVA, normality of residuals was assessed using the Shapiro–Wilk test ( $W \geq 0.90$ ,  $p > 0.05$  for all properties; note: Hardness groups UT and NT returned degenerate Shapiro–Wilk results owing to tied values at  $n = 3$ , and normality for those groups is considered inconclusive), and homogeneity of variance was evaluated using Levene's test ( $p > 0.05$  for all properties), indicating that the assumptions for parametric testing were reasonably satisfied. To contextualise the practical significance of the observed differences, partial eta-squared ( $\eta^2$ ) effect sizes were calculated for each property, and Cohen's  $d$  values were computed for selected pairwise comparisons. Given the limited sample size ( $n = 3$  per group), all statistical conclusions are interpreted cautiously, and the results are used to identify comparative performance trends rather than to establish definitive material property values.

### 2.11 Regression-based response modelling

Regression analysis used specimen-level mechanical responses ( $n = 9$ ) from rPET–jute composites reinforced with untreated (UT), NaOH-treated (NT), and silane-treated (ST) fibres (three specimens per condition). Neat rPET was excluded from the modelling analysis, as it does not contain fibre–matrix interfaces and therefore lacks a meaningful porosity–interface relationship. porosity ( $P$ ) was taken as the condition-wise mean porosity, calculated from the mean density ( $\rho_c$ ) and the constant theoretical density ( $\rho_i$ ), and then assigned to the three specimens within each condition for modelling. Accordingly, the predictor contained three discrete porosity levels, whereas the response variables retained specimen-level scatter.

Because porosity is computed directly from experimental density,  $\rho_c$  and  $P$  are mathematically dependent. Including both as independent predictors would introduce perfect multicollinearity. Therefore, a single-predictor linear regression model using porosity ( $P$ ) was adopted to ensure statistical validity and interpretability. Four mechanical

responses—tensile strength, flexural strength, short-beam shear strength (SBSS), and hardness—were considered as outputs.

The linear regression model was expressed as:

$$Y = \beta_0 + \beta_1 P \quad (8)$$

where  $Y$  represents the mechanical response,  $P$  is porosity (%), and  $\beta_0$  and  $\beta_1$  are the intercept and slope coefficients determined by least-squares fitting. This regression analysis served as a parsimonious structure–property model to quantify the influence of densification on mechanical performance within the experimental porosity domain (2.4–3.9%).

To assess predictive robustness, Leave-One-Out Cross-Validation (LOOCV) was applied to the regression models. In LOOCV, each of the nine specimens is withheld in turn, the model is re-fitted on the remaining eight observations, and the withheld specimen is predicted. The cross-validated coefficient of determination was calculated as:

$$R_{CV}^2 = 1 - \frac{\sum (y_i - \hat{y}_{i,cv})^2}{\sum (y_i - \bar{y})^2} \quad (9)$$

where  $\hat{y}_{i,cv}$  denotes the out-of-sample prediction for specimen  $i$ , and  $\bar{y}$  is the global mean of the full response vector. Using the global mean baseline ensures consistency with standard LOOCV practice and allows direct comparison with training  $R^2$  values.

## 2.12 Life Cycle Assessment (LCA) Methodology

A cradle-to-gate life cycle assessment (LCA) was conducted to evaluate the environmental impacts associated with the production of rPET–jute composites reinforced with untreated (UT), NaOH-treated (NT), and silane-treated (ST) fibres. The assessment focused on global warming potential (GWP, kg CO<sub>2</sub>-eq) as the selected impact category. The methodological framework followed the principles of ISO 14040 and ISO 14044, including goal and scope definition, life-cycle inventory compilation, impact assessment, and interpretation. All calculations were performed using a custom Python-based calculation framework implemented in the Spyder Integrated Development Environment (IDE) within Anaconda 2024 (Python 3.11 environment).

The functional unit was defined as 1 kg of finished composite material, enabling direct comparison among the three fibre-treatment conditions. The system boundary was defined as cradle-to-gate and included: (i) collection and preparation of post-consumer PET water bottles, (ii) washing, shredding, and pelletising of recycled PET, (iii) jute fibre extraction and surface modification, (iv) melt compounding using a twin-screw extruder, and (v) injection moulding of the composite specimens. The use phase and end-of-life stages were excluded, as the objective of this study was to evaluate manufacturing-stage environmental impacts associated with recycled composite production.

Experimentally measured material compositions were used directly as model inputs. Each composite formulation consisted of 80 wt% rPET and 20 wt% jute fibre. The experimentally produced specimen mass (approximately 50 g) was linearly scaled to the 1 kg functional unit. Fibre surface-treatment inputs were modelled based on laboratory-scale consumption, including approximately 5 g NaOH for alkali treatment and an additional

3 g silane coupling agent for the ST condition. These quantities were proportionally scaled to the functional unit and incorporated into the life-cycle inventory.

Energy consumption for extrusion and injection moulding was included using standard laboratory-scale values representative of small-batch composite processing. Energy requirements of 1.8 kWh/kg for extrusion [28] and 1.2 kWh/kg for injection moulding [29] were adopted based on reported values in recent material processing LCAs [30]. The cradle-to-gate emission factor for rPET was set to 0.45 kg CO<sub>2</sub>-eq/kg, consistent with published LCA inventory data for rPET feedstock production [31, 32] (see Supplementary Table S1 for full inventory inputs and emission factors). All experimental processing was conducted in Chennai, India; therefore, electricity-related emissions were calculated using an India-specific Combined Margin grid emission factor of 0.71 kg CO<sub>2</sub>-eq kWh<sup>-1</sup>, based on the Central Electricity Authority (CEA), CO<sub>2</sub> Baseline Database for the Indian Power Sector [33]. To evaluate sensitivity to grid intensity assumptions, an alternative lower-intensity scenario was also assessed.

Energy consumption for bottle washing, shredding, and pelletisation was not directly metered and is therefore not explicitly included in the base-case model. This limitation is acknowledged as part of the screening-level, laboratory-scale cradle-to-gate estimation. Chemical treatment energy was assumed negligible, as fibre modification was performed at room temperature without active heating. Transportation impacts were included using a default distance of 50 km for raw material transport, representing local recycling and fibre supply conditions.

The total GWP was calculated using a deterministic mass–energy summation model:

$$\text{Total GWP} = \sum (m_i \times EF_i) + (\text{Electricity} \times EF_{\text{grid}}) + \text{Transport} \quad (10)$$

where  $m_i$  represents the mass of each material input and  $EF_i$  its corresponding emission factor expressed in kg CO<sub>2</sub>-eq per unit mass,  $E_{\text{electricity}}$  is the total electricity consumption (kWh), and  $EF_{\text{grid}}$  is the grid emission factor. All emission factors were applied directly in 100-year GWP (GWP100) terms. Supplementary information is available and includes the life-cycle inventory (Table S1) and analysis scripts/data used for regression/LOOCV and LCA calculations.

The Python script calculated total CO<sub>2</sub>-equivalent emissions by summing contributions from raw materials, fibre-treatment chemicals, transport, and processing electricity. The script functions solely as a transparent computational tool based on referenced emission factors and does not constitute an independent LCA database. Separate scenarios were generated for UT, NT, and ST composites, enabling clear comparison of the environmental implications of increasing fibre-treatment intensity. The Spyder-based framework allowed transparent parameter definition, direct integration of experimentally measured data, and rapid sensitivity analysis without reliance on specialist commercial LCA software.

Sensitivity analysis was conducted by varying electricity-related emissions by  $\pm 30\%$  relative to the baseline grid emission factor. This scenario evaluation was implemented parametrically within the Python framework to assess the robustness of comparative conclusions under different electricity carbon-intensity assumptions. The resulting model outputs provide quantitative insight into the environmental trade-offs between fibre surface modification and mechanical property enhancement, thereby supporting

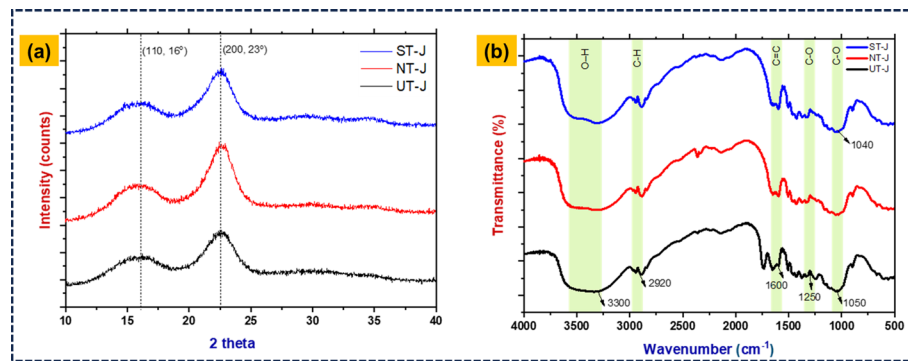


**Fig. 2** (a) XRD pattern and (b) FTIR spectra of untreated, NaOH-treated, and silane-treated jute fibres

**Table 1** Crystallinity index (CI) and crystallite size (D) of jute fibre

Fibre	$I_{200}$ (counts)	$I_{AM}$ (counts)	CI (%)	D (nm)
UT-J	54.50	26.53	51.3	4.02
NT-J	68.77	26.25	61.8	4.51
ST-J	60.08	26.03	56.7	4.50

the broader objective of developing mechanically improved yet environmentally responsible recycled polymer composites.

### 3 Results and discussion

#### 3.1 XRD and FTIR

The XRD patterns of UT-J, NT-J, and ST-J jute fibres are presented in Fig. 2a and the CI and D values for all three fibre conditions are presented in Table 1. All three fibres display characteristic cellulose I peaks at  $2\theta \approx 15.8^\circ$  ((1-10)/(110)) and  $22.4^\circ$  (200) along with a weak reflection near  $34.5^\circ$  (004), confirming the retention of the native cellulose I polymorph across all treatment conditions. The untreated fibre (UT-J) exhibits a broad, low-intensity (200) peak, indicating a mixed amorphous–crystalline structure with considerable presence of hemicellulose and lignin. The amorphous hump between  $16\text{--}19^\circ$  reflects significant disorder in the cellulose network, yielding the lowest crystallinity index (CI=51.3%) and the smallest crystallite size ( $D=4.02$  nm) among the three fibre conditions (Table 1). After NaOH treatment (NT-J), the (200) peak becomes markedly sharper and more intense, while the amorphous hump weakens substantially, signifying removal of non-cellulosic surface constituents and rearrangement of cellulose microfibrils into a more ordered packing. This structural reorganisation produces the highest CI of 61.8% and the largest crystallite size ( $D=4.51$  nm), reflecting stronger intermolecular hydrogen bonding and tighter fibril alignment. The silane-treated sample (ST-J) retains a sharp (200) reflection with an intermediate CI of 56.7% and a crystallite size ( $D=4.50$  nm) essentially identical to that of NT-J. The slight reduction in CI relative to NT-J is consistent with the mechanism of silane treatment: the coupling agent functionalises the hydroxyl-rich fibre surface through Si–O–C bond formation, improving surface orientation and reducing moisture adsorption, but without the bulk delignification achieved by NaOH and therefore without the same degree of crystalline enrichment. Importantly, no new crystalline peaks appear in the ST-J pattern, confirming that the silane treatment preserves the cellulose I polymorph without inducing polymorphic transformation. The CI and D values for all three fibre conditions, determined from

Segal's method and the Scherrer equation respectively, are compiled in Table 1. Overall, the trend  $UT-J < ST-J < NT-J$  in CI, alongside the overall increase in D from 4.02 nm (UT-J) to 4.51 nm (NT-J), reflects the mechanistically distinct roles of the two treatments: alkali treatment acts on the bulk fibre by stripping hemicellulose and lignin, while silane treatment operates primarily at the fibre surface, functionalising exposed hydroxyl groups without comparable bulk crystalline reorganisation.

The FTIR spectra of untreated (UT-J), alkaline-treated (NT-J), and silane-coupled (ST-J) jute fibres, shown in Fig. 2b, reveal systematic chemical transformations arising from the sequential surface-modification treatments. The untreated jute fibre exhibits characteristic absorption bands at  $\sim 3300\text{ cm}^{-1}$  (O–H stretching of hydroxyl groups),  $\sim 2920\text{ cm}^{-1}$  (C–H stretching of aliphatic chains),  $\sim 1600\text{ cm}^{-1}$  (aromatic C=C stretching of lignin), and  $\sim 1050\text{ cm}^{-1}$  (C–O–C glycosidic vibrations of cellulose), consistent with the intact multiphase composition of cellulose, hemicellulose, and lignin. Following alkaline treatment with NaOH, the marked reduction of the lignin-characteristic band at  $\sim 1600\text{ cm}^{-1}$  indicates the efficient removal of amorphous lignin and hemicellulose components from the fibre surface. Concurrently, the enhanced relative intensity of the cellulose-associated peak at  $\sim 1050\text{ cm}^{-1}$  in the NT-J spectrum compared to UT-J demonstrates increased cellulose purity and accessibility due to partial delignification and dehemicellulization. In contrast, the silane-coupled ST-J sample exhibits distinct spectral changes characteristic of successful surface functionalization. A pronounced enhancement around  $\sim 1040\text{ cm}^{-1}$ , corresponding to overlapping Si–O–Si stretching vibrations from the siloxane network and cellulose C–O–C bonds, is consistent with the formation of covalent siloxane linkages on the jute fibre surface. The broad increase in absorbance within the  $1000\text{--}1200\text{ cm}^{-1}$  region further reflects the development of a condensed siloxane layer during the silane grafting process. Importantly, the retention of the characteristic cellulose bands and the absence of any new degradation-related absorptions suggest that the silane treatment preserves the structural integrity of the underlying cellulose framework. Overall, these FTIR findings support the interpretation that sequential alkaline and silane treatments effectively remove non-cellulosic constituents, enrich cellulose crystallinity, and introduce a reactive siloxane interphase on the fibre surface. This dual modification not only enhances the chemical purity of jute fibres but also establishes a robust interfacial bridge, promoting improved adhesion and stress transfer in polymer composite systems.

### 3.2 Density and porosity analysis

The theoretical and experimental densities of the rPET–jute composites, together with the calculated porosity, are presented in Table 2. The theoretical density remained almost constant at  $1.27\text{ g/cm}^3$  for all composites, as it depended on the known proportions of fibre and matrix used during fabrication. In contrast, the experimental density varied slightly with surface treatment, increasing from  $1.22\text{ g/cm}^3$  for the UT composite to  $1.23\text{ g/cm}^3$  for the NT and  $1.24\text{ g/cm}^3$  for the ST composite. This steady increase

**Table 2** Density and porosity of rPET–jute composites

Composite Sample	$\rho_t$ ( $\text{g/cm}^3$ )	$\rho_e$ ( $\text{g/cm}^3$ )	Porosity (%)
UT	1.27	1.22	3.9
NT	1.27	1.23	3.1
ST	1.27	1.24	2.4

in measured density indicated improved fibre–matrix compaction after surface modification. The calculated porosity decreased significantly from 3.9% (UT) to 3.1% (NT) and 2.4% (ST). The higher porosity in the untreated composite was mainly due to poor interfacial bonding and fibre surface impurities such as wax and lignin, which trapped air pockets during injection moulding. Alkali treatment partially removed these impurities and enhanced fibre roughness, allowing better matrix wetting and reduced void formation. The lowest porosity observed in the silane-treated composite reflected a more uniform and compact microstructure resulting from strong interfacial adhesion and chemical bonding between the fibre and matrix.

The progressive decrease in porosity and increase in experimental density with surface modification reflected a denser and more uniform composite structure. Similar observations were made by Ramamoorthy et al. [34], it was reported that effective fibre surface treatment reduced void content and improved matrix infiltration in natural fibre–reinforced polymers. These findings suggest that both alkali and silane treatments contributed to improved structural consolidation and reduced internal defects in the rPET–jute composites.

### 3.3 Mechanical properties

The mechanical properties of the rPET–jute composites reinforced with UT, NT, and ST fibres were compared with those of the neat rPET matrix. The results revealed a consistent improvement across all measured parameters—tensile strength, flexural strength, SBSS, and hardness—following fibre surface treatment.

#### 3.3.1 Tensile Behaviour of rPET–Jute Fibre Composites

The tensile properties of the neat and fibre-reinforced rPET composites are shown in Fig. 3. The results indicated a clear improvement in strength and stiffness with fibre surface treatment, reflecting better bonding and load transfer between the jute fibres and the rPET matrix. The neat rPET showed a mean tensile strength of 32.08 MPa, which represents the base strength of the recycled polymer without reinforcement. When untreated jute fibres were added, the tensile strength increased to 38.78 MPa, giving a rise of about 20.9%. This improvement was mainly due to the higher stiffness of the jute fibres, which limited the deformation of the polymer under load. However, the untreated fibres still contained surface impurities such as waxes, lignin, and hemicellulose, which reduced adhesion with the matrix. This weak interfacial bonding led to fibre pull-out

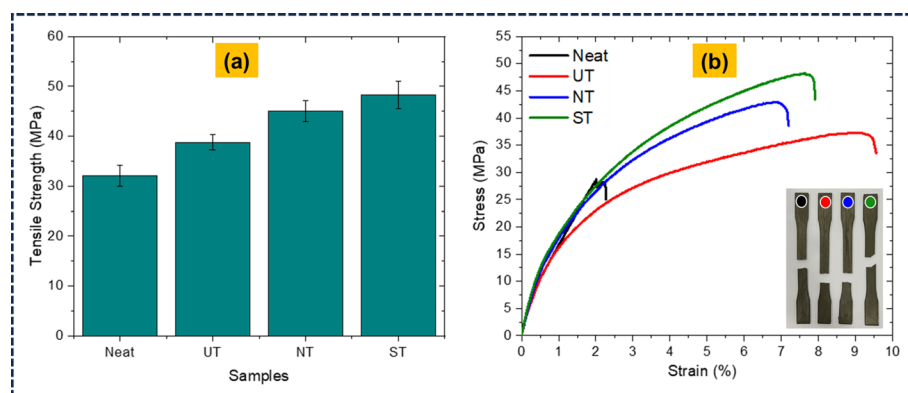


**Fig. 3** (a) Tensile strength and (b) stress–strain curves of rPET–jute composites

and poor stress transfer, causing premature fracture, as reflected by the lower slope and reduced elongation in the stress–strain curve. After alkali treatment, the tensile strength increased to 45.02 MPa, around 40.3% higher than the neat matrix. The NaOH treatment removed amorphous surface components, exposing cellulose microfibrils and increasing surface roughness [35, 36]. This improved the wettability and interlocking between the fibre and matrix. The stress–strain curve of the NaOH-treated composite showed a longer linear region, indicating a higher elastic limit and more uniform stress distribution before failure. The density results supported this trend, showing that NaOH-treated composites (density = 1.23 g/cm<sup>3</sup>) had lower porosity (3.1%) than untreated ones (3.9%), suggesting improved packing and reduced void formation, which in turn aided better stress transfer.

The ST composite showed the highest tensile strength of 48.29 MPa, representing a 50.5% improvement over the neat matrix and 24.5% over the untreated composite. The silane coupling promoted chemical bonding between hydroxyl groups on the fibre surface and functional groups of the silane, forming Si–O–C and Si–O–Si linkages. These bonds strengthened the interfacial region, reduced microvoids, and delayed crack propagation under tension [18]. The stress–strain curve of the ST composite displayed the steepest slope and highest yield point, suggesting increased stiffness and interfacial stability. This improvement was in line with the higher density (1.24 g/cm<sup>3</sup>) and the lowest porosity (2.4%), indicating a denser and more compact structure that provided effective load transfer during tensile loading. The improvement trend of ST > NT > UT > Neat was consistent across all samples, suggesting that combined alkali and silane treatment was most effective in promoting strong interfacial bonding and efficient stress distribution between the fibre and polymer. These results agree well with earlier studies by Hong et al. [37] for silane-modified jute fibre PP composites. It can therefore be concluded that surface treatment of jute fibres had a major influence on the tensile performance of rPET composites. The improved behaviour was closely linked with the observed reduction in porosity and increase in experimental density, suggesting better structural integrity and bonding. The removal of impurities, increased roughness, and formation of chemical linkages promoted efficient stress transfer and reduced early fibre pull-out.

### 3.3.2 Flexural and Short Beam Shear Behaviour of rPET–Jute Fibre Composites

The flexural and short beam shear test (SBSS) results are presented in Fig. 4. Fibre surface modification had a strong influence on the bending and interfacial performance of

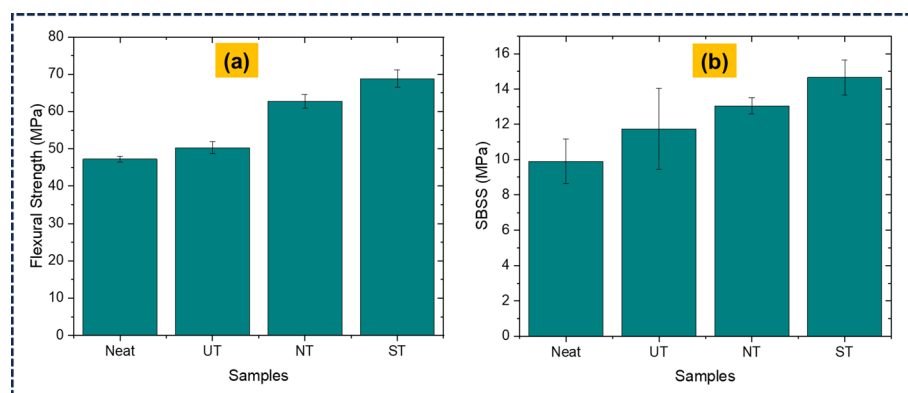


**Fig. 4** Flexural strength and SBSS of rPET–jute composites

the rPET–jute composites, showing a trend consistent with but distinct from the tensile results. Both flexural strength and SBSS increased progressively from the neat rPET to the ST composite, suggesting that surface treatment improved stress transfer across the fibre–matrix interface and reduced failure at the interphase during bending and shear loading. The neat rPET exhibited a flexural strength of 47.24 MPa, typical of a ductile thermoplastic with limited bending resistance. The addition of untreated jute fibres slightly increased this value to 50.30 MPa, an improvement of about 6.5%. The increase was mainly attributed to the inherent stiffness of jute fibres, which limited matrix deformation. However, incomplete wetting and the presence of surface impurities led to fibre debonding and crack initiation under flexural stress, preventing further improvement. After alkali treatment, the flexural strength increased markedly to 62.78 MPa, which was 32.9% higher than the neat polymer. The NaOH treatment removed waxy layers, lignin, and hemicellulose from the fibre surface, resulting in a rougher texture that promoted better mechanical interlocking and adhesion. This enhanced bonding enabled more uniform stress distribution and delayed delamination under bending. The higher experimental density ( $\rho_e = 1.23 \text{ g/cm}^3$ ) and lower porosity (3.1%) observed in the NT composite supported this behaviour, indicating a more compact structure with reduced voids.

The ST composite achieved the highest flexural strength of 68.84 MPa, representing improvements of 45.7% over the neat matrix and 36.9% over the untreated composite. The silane coupling agent acted as a chemical bridge between the hydroxyl-rich jute fibre surface and the rPET matrix, forming Si–O–Si and Si–O–C bonds that enhanced interfacial adhesion and compatibility. This chemical bonding reduced microvoids, increased fibre anchoring, and delayed crack propagation, which collectively improved bending resistance. The slight rise in  $\rho_e$  ( $1.24 \text{ g/cm}^3$ ) and the lowest porosity (2.4%) further supported the improved interfacial consolidation and compact microstructure.

A consistent improvement trend was also observed for SBSS. The neat rPET showed an SBSS of 9.90 MPa, which increased to 11.74 MPa for UT (+18.6%), 13.05 MPa for NT (+31.8%), and 14.66 MPa for ST (+48.1%). This steady rise is consistent with the interpretation that surface treatment improved shear load transfer and reduced interfacial slippage. The NT composite exhibited improved adhesion due to the removal of weak boundary layers, while the ST composite showed the strongest interface, attributed to covalent bonding between silane and cellulose hydroxyl groups. The reduced porosity and increased density observed for these treated composites correlated with their higher SBSS, indicating a denser interphase and stronger bonding. The overall order  $ST > NT > UT > \text{Neat}$  reflected the gradual improvement in interfacial integrity with treatment. The reduction of voids and improved matrix infiltration supported stronger interfacial bonding and more stable shear response.

### 3.3.3 Fracture analysis

To further understand the failure behaviour associated with the mechanical results, scanning electron microscopy (SEM) was carried out on fractured specimens after mechanical testing. Representative images of neat rPET, the untreated fibre composite (UT), and the NaOH-treated composite (NT) are shown in Fig. 5. The fracture surface of neat rPET (Fig. 5(a)) showed a relatively smooth appearance with limited fibrillation and little crack deflection. This type of morphology is typical of semi-crystalline PET, where failure mainly occurs through crack initiation and growth within the polymer matrix.

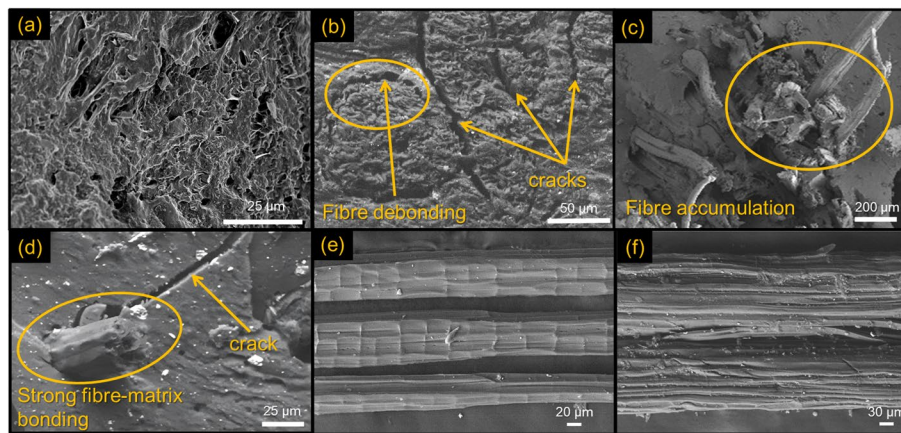


**Fig. 5** SEM fracture surfaces of (a) neat rPET, (b) UT composite showing interfacial debonding and cracks, (c) NT composite showing fibre pull-out and matrix deformation, and (d) ST composite exhibiting strong fibre–matrix bonding; (e) untreated jute fibre surface and (f) NaOH-treated jute fibre surface

Energy absorption mechanisms were therefore limited, and the fracture was largely controlled by the matrix behaviour. In contrast, the UT composite (Fig. 5(b)) showed clear signs of fibre–matrix debonding and crack growth along the fibre surface. Gaps were visible around several embedded fibres, indicating weak interfacial bonding. These features suggest that stress transfer between the hydrophilic jute fibres and the rPET matrix was not fully effective. Similar interfacial debonding has been reported in untreated natural fibre thermoplastic composites, where poor adhesion leads to early crack formation and reduced load transfer efficiency. The presence of interfacial voids and crack coalescence in the UT specimens is consistent with the lower tensile and short-beam shear strength values measured for this condition. Although severe crack formation was not observed in the NT and ST composites, localised fibre accumulation and fibre pull-out were evident in several regions. The NT composite (Fig. 5(c)) showed reduced interfacial separation compared with UT, together with matrix deformation around the pulled-out fibres. Alkali treatment removes surface components such as hemicellulose, lignin, and waxes. This process increases surface roughness and exposes cellulose hydroxyl groups on the fibre surface. As a result, mechanical interlocking between the fibre and the matrix can improve. The features observed in Fig. 5(c) indicate closer fibre–matrix contact in the NT specimens compared with the untreated composite. Figure 5(d) further shows regions of strong fibre–matrix bonding in the ST fibre composite, where fibre fracture rather than pull-out is observed, along with cracks propagating through the matrix. This indicates improved interfacial adhesion and more effective stress transfer between the fibre and matrix. In both NT and ST conditions, the modified fibre surfaces likely reduced interfacial separation, improved wetting of the fibre by the polymer melt, and limited crack growth along the interface. These interfacial changes support more efficient stress transfer from the matrix to the fibres. The higher tensile, flexural, and shear strengths measured for the NT and ST composites are therefore consistent with the improved interfacial interaction achieved through alkali and silane treatments.

### 3.3.4 Hardness Behaviour of rPET–Jute Fibre Composites

The hardness results of the rPET–jute composites are presented in Fig. 6. The hardness increased gradually with fibre addition and surface treatment, indicating that

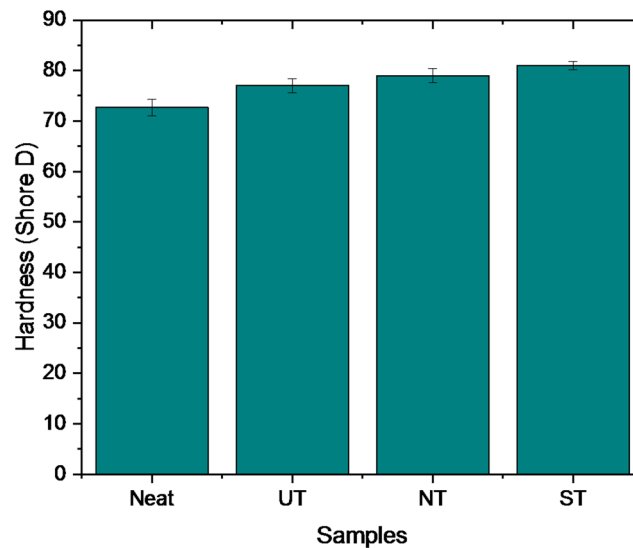


**Fig. 6** Hardness of rPET-jute composites

the presence of well-bonded fibres restricted local deformation of the polymer during indentation. The neat rPET showed a hardness value of 72.67 Shore D, further incorporation of untreated jute fibres increased the hardness to 77.00 Shore D, an improvement of about 6%. This increase was mainly due to the higher stiffness of the jute fibres, which reduced matrix mobility during the indentation process. However, the interface between untreated fibres and the polymer was weak, and small interfacial voids likely caused non-uniform load transfer, limiting the improvement. The NaOH-treated composite exhibited a higher hardness of 79.00 Shore D, showing an 8.7% increase compared with the neat sample. The alkali treatment removed impurities and exposed cellulose microfibrils on the fibre surface, which led to better mechanical anchoring with the polymer matrix. The improved interlocking reduced the tendency for local yielding of the matrix near the fibre-polymer interface. Similar effects were reported by Rajeshkumar et al. [38], it was found that alkali-treated *Bauhania Purpurea L* fibre epoxy composites displayed higher surface rigidity due to improved fibre-matrix contact.

The ST composite showed the highest hardness of 81.00 Shore D, representing an 11.45% increase over the neat rPET. The improvement was mainly attributed to chemical bonding between the silane coupling agent and the hydroxyl groups of cellulose, forming Si-O-Si and Si-O-C linkages. These bonds provided a strong interfacial region that enhanced load transmission and reduced indentation-induced deformation. The dense fibre-matrix network also restricted the local movement of polymer chains, producing a stiffer and more compact structure. The consistent increase across the UT, NT, and ST samples suggested that both physical roughness and chemical compatibility contributed to the surface strengthening of the composites. The result trend followed  $ST > NT > UT > Neat$ , which is consistent with the view that combined alkali and silane treatment was the most effective approach for improving surface hardness. The treated fibres limited plastic deformation of the polymer during indentation and enhanced local stiffness through stronger interfacial bonding. These improvements indicate that surface-engineered jute fibres can effectively increase the wear and indentation resistance of recycled polymer composites, improving their potential for use in structural and semi-structural applications.

**Table 3** ANOVA for mechanical properties of rPET–jute composites

Property	F-statistic	p-value	Significance ( $\eta^2$ ) ( $\alpha = 0.05$ )	Best Performer (Mean)	Lowest Performer (Mean)
Tensile Strength	22.11	0.0003	Yes (0.89)	ST (48.29 MPa)	Neat (32.08 MPa)
SBSS	10.28	0.004	Yes (0.79)	ST (14.66 MPa)	Neat (9.90 MPa)
Flexural Strength	68.76	< 0.0001	Yes (0.96)	ST (68.84 MPa)	Neat (47.24 MPa)
Hardness	13.44	0.002	Yes (0.83)	ST (81.00)	Neat (72.67)

**Table 4** Tukey HSD pairwise comparison summary ( $p < 0.05$ )

Property	Significant Pairs	Statistical Effect	Interpretation
Tensile Strength	Neat ↔ NT	Significant improvements over Neat for NT and ST treatments; UT ↔ ST also significant	ST composites exhibited the highest tensile strength due to optimal interfacial coupling
	Neat ↔ ST		
	UT ↔ ST		
SBSS	Neat ↔ NT	Significant improvements over Neat for NT and ST treatments; UT ↔ ST also significant	Silane coupling significantly enhanced fibre–matrix adhesion
	UT ↔ ST		
Flexural Strength	Neat ↔ NT	Significant improvements across most pairs; only Neat ↔ UT not significant	Maximum flexural strength observed in ST composites
	UT ↔ ST		
	NT ↔ ST		
Hardness	Neat ↔ NT	Only Neat ↔ NT and Neat ↔ ST significant; adjacent-treatment differences not significant	Progressive densification and load-bearing surface integrity with treatment
	Neat ↔ ST		
	—		

### 3.4 One-Way ANOVA and Tukey HSD Post-Hoc Analysis

A one-way ANOVA was conducted for each mechanical property to examine the influence of fibre surface treatment on the rPET–jute composites. As summarised in Table 3, all F-statistics exceeded the critical threshold ( $F > 3.11$ ) with  $p < 0.05$ , indicating that fibre treatment had a statistically significant effect on the strength, stiffness, and hardness of the composites.

The subsequent Tukey HSD post-hoc analysis (Table 4) identified specific group pairs contributing to these differences. ST composites consistently exhibited superior performance in tensile, SBSS, flexural, and hardness properties, followed by NT and UT composites. The improvements in the ST group were attributed to enhanced interfacial bonding facilitated by silane coupling, resulting in more efficient stress transfer and reduced interfacial defects.

The ANOVA and Tukey HSD analyses indicate that all measured properties were significantly influenced by surface treatment ( $p < 0.05$ ). The tensile and flexural strengths of the silane-treated composites (48.29 MPa and 68.84 MPa, respectively) showed notable improvements of 50.5% and 45.7% over the neat matrix. Similarly, SBSS and hardness increased by 48% and 11.45%, respectively, consistent with enhanced fibre–matrix bonding. These statistical outcomes align closely with the experimental findings, supporting the interpretation that chemical and silane surface treatments effectively reinforced the interfacial performance of rPET–jute composites. The Tukey HSD post-hoc analysis (Table 3) showed that statistically significant pairwise differences were concentrated in larger treatment-step comparisons (Neat ↔ NT, Neat ↔ ST, and UT ↔ ST across most properties), while most adjacent-step pairs were not significant at  $n = 3$ . Large effect sizes ( $\eta^2 = 0.79–0.96$ ) indicate that fibre treatment explained a substantial proportion of the total variance; these results are best interpreted as establishing comparative performance trends rather than definitive material property values. In particular, the hardness

trends while statistically significant according to ANOVA ( $p < 0.05$ ,  $\eta^2 = 0.83$ ) should be interpreted as preliminary comparative indicators rather than definitive material constants, given the inconclusive Shapiro–Wilk normality results for the UT and NT groups arising from tied values at  $n = 3$ .

### 3.5 Regression-Based Response Modelling

The regression analysis revealed a consistent and physically meaningful relationship between porosity (P) and the mechanical properties of the rPET–jute composites. Because  $\rho_c$  and P are mathematically dependent (porosity is computed directly from experimental density), a single-predictor model using porosity was adopted to avoid multicollinearity. For all four properties, the regression slope coefficients were negative, indicating that reduced porosity corresponded to improved tensile strength, flexural strength, short-beam shear strength (SBSS), and hardness. The derived regression equations are presented in Table 5. In each case, the ST composite, which exhibited the lowest porosity (2.4%), showed the highest predicted mechanical performance, consistent with the experimental observations.

The multiple linear regression (MLR) model achieved  $R^2$  values of 0.631–0.916 (adjusted  $R^2$ : 0.578–0.904) and MAPE values of 1.44–4.66% across the four properties. Flexural strength exhibited the strongest linear dependence on porosity ( $R^2 = 0.916$ ; adjusted  $R^2 = 0.904$ ), while hardness showed the weakest ( $R^2 = 0.631$ ; adjusted  $R^2 = 0.578$ ). The adjusted  $R^2$  values account for the limited sample size ( $n = 9$ ) and indicate that the models remain internally consistent within the experimental domain.

The predicted versus experimental plots (Fig. 7) demonstrate reasonable alignment across all properties, supporting the adequacy of the single-predictor regression model within the investigated porosity range (2.4–3.9%). Given that only three discrete porosity levels were experimentally examined (UT, NT, ST), the use of higher-order polynomial models would not be statistically justified and could introduce artificial curvature unsupported by the data. The moderate  $R^2$  values should be interpreted in the context of specimen-level mechanical scatter, which inherently reduces model fit relative to group-mean trends.

To assess predictive robustness, Leave-One-Out Cross-Validation (LOOCV) was performed. Cross-validated  $R^2$  values were 0.576 (tensile strength), 0.861 (flexural strength), 0.503 (SBSS), and 0.391 (hardness), indicating that the training metrics were not severely inflated and that the observed relationships are not artefacts of overfitting. Flexural strength retained strong cross-validated predictability, consistent with the known sensitivity of bending performance to void distribution. Tensile strength and SBSS exhibited moderate cross-validated performance ( $R^2 \approx 0.50$ – $0.58$ ), indicating that while porosity is a dominant factor, interfacial bonding mechanisms not fully captured by bulk porosity also contribute. Hardness showed the weakest cross-validated dependence ( $R^2 = 0.391$ ), reflecting its greater sensitivity to surface chemistry rather than bulk void content.

**Table 5** Derived regression equations and performance indicators ( $n = 9$  specimens)

Property	Regression Equation	$R^2$	MAPE (%)	$R^2_{adj}$
Tensile Strength	$Y = -6.37P + 64.00$	0.749	4.23	0.714
Flexural Strength	$Y = -12.44P + 99.61$	0.916	3.18	0.904
SBSS	$Y = -1.94P + 19.22$	0.725	4.66	0.686
Hardness	$Y = -2.66P + 87.34$	0.631	1.44	0.578

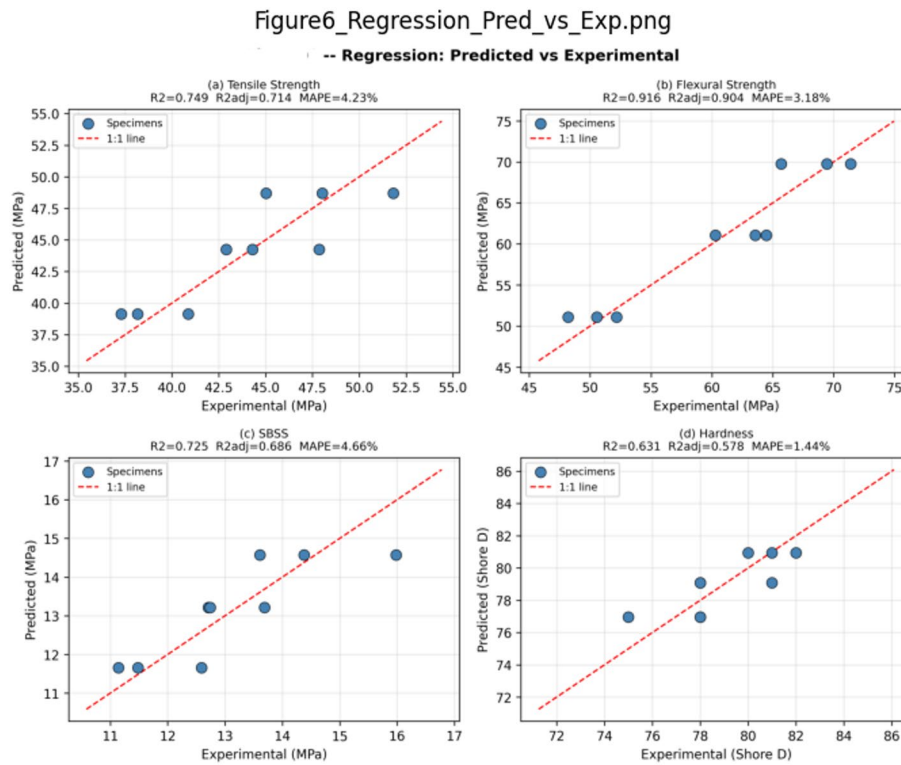


**Fig. 7** Comparison of experimental and predicted mechanical properties using the regression model: (a) Tensile strength, (b) Flexural strength, (c) SBSS, (d) Hardness

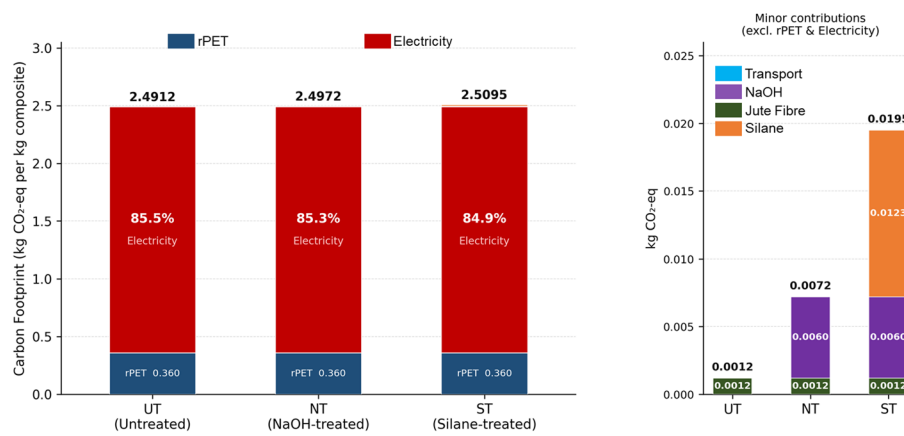


**Fig. 8** Carbon footprint of rPET jute composites

### 3.6 Life Cycle Assessment (LCA) Results

The cradle-to-gate LCA quantified the carbon footprint associated with the production of 1 kg-equivalent rPET–jute composite for all three–fibre surface-treatment conditions (UT, NT, and ST). The results are summarised in Fig. 8; Table 6. The total carbon footprint values were low and closely grouped, ranging from 2.49 to 2.51 kg CO<sub>2</sub>-eq, indicating that fibre surface modification introduces only a marginal additional environmental burden relative to untreated fibre composites under the defined laboratory-scale processing conditions. The UT composite exhibited a total carbon footprint of 2.4912 kg CO<sub>2</sub>-eq, with electricity consumption during twin-screw compounding and injection

**Table 6** Detailed LCA breakdown (kg CO<sub>2</sub>-eq per functional unit)

Composite	Total CF	Electricity	rPET	Jute Fibre	NaOH	Silane	Transport
UT	2.4912	2.1300	0.3600	0.0012	0.0000	0.0000	0.0000
NT	2.4972	2.1300	0.3600	0.0012	0.0060	0.0000	0.0000
ST	2.5095	2.1300	0.3600	0.0012	0.0060	0.0123	0.0000

Transport contribution =  $(1 \text{ kg} / 1000) \times 50 \text{ km} \times 0.0002 \text{ kg CO}_2\text{-eq tonne}^{-1} \text{ km}^{-1} = 0.00001 \text{ kg CO}_2\text{-eq}$ ; displayed as 0.0000 at four decimal places

moulding contributing 2.1300 kg CO<sub>2</sub>-eq (approximately 85.5%). Contributions from rPET flakes were 0.3600 kg CO<sub>2</sub>-eq (EF=0.45 kg CO<sub>2</sub>-eq kg<sup>-1</sup>, mechanical recycling, cradle-to-gate) and raw jute fibre contributing 0.0012 kg CO<sub>2</sub>-eq, highlighting the low embodied carbon of recycled plastics and natural fibres. Transport impacts were negligible (0.00001 kg CO<sub>2</sub>-eq; shown as 0.0000 in Table 6).

For the NT composite, the carbon footprint increased slightly to 2.4972 kg CO<sub>2</sub>-eq, primarily due to the addition of NaOH used during fibre modification (0.0060 kg CO<sub>2</sub>-eq). This corresponds to an increase of approximately 0.24% relative to UT, indicating that alkali treatment introduces only a minor environmental penalty while enabling substantial improvements in tensile strength, flexural strength, and short-beam shear performance. The ST composite showed the highest carbon footprint (2.5095 kg CO<sub>2</sub>-eq), reflecting the combined contribution of NaOH and silane coupling agent. The silane treatment contributed an additional 0.0123 kg CO<sub>2</sub>-eq, resulting in an overall increase of approximately 0.73% compared with UT. Despite this increase, the absolute environmental impact remains small relative to the experimentally observed enhancements in mechanical properties, suggesting a favourable performance-to-impact balance for surface-modified composites.

Across all composite variants, electricity consumption was the dominant contributor, accounting for approximately 84.9–85.5% of total emissions. Material-related contributions (rPET, jute fibre, and treatment chemicals) accounted for approximately 14.5–15.1% of total GWP, while transport impacts remained negligible (0.00001 kg CO<sub>2</sub>-eq, shown as 0.0000 in Table 6), consistent with the assumption of local raw-material sourcing. These findings indicate that the environmental profile of rPET–jute composites is governed primarily by manufacturing energy demand rather than fibre treatment intensity. It should be noted that the electricity-related emissions reflect laboratory-scale processing energy intensity and the use of a grid-average emission factor. Laboratory-scale processing often exhibits lower energy efficiency than industrial-scale production; therefore, the reported carbon footprint values should be interpreted as screening-level cradle-to-gate estimates rather than full industrial lifecycle burdens. To evaluate the robustness of these results, a sensitivity analysis was conducted by varying electricity-related emissions by  $\pm 30\%$ . As expected, the absolute global warming potential (GWP) showed strong dependence on electricity consumption, ranging from approximately 1.85 to 3.15 kg CO<sub>2</sub>-eq per kg of composite. However, the relative ranking of the composites remained unchanged across all scenarios (UT < NT < ST), and the incremental contribution of fibre surface treatments remained marginal. This indicates that, although absolute carbon footprint values are sensitive to energy assumptions, the comparative conclusions regarding fibre-treatment effects are robust. Overall, the LCA results demonstrate that the modest increase in carbon footprint associated with fibre surface treatment is substantially outweighed by the significant mechanical performance improvements achieved. The integration of surface-engineered natural fibres into

recycled PET therefore represents a mechanically effective and environmentally responsible strategy for sustainable thermoplastic composite development.

It should be noted that the reported carbon footprint values represent a screening-level, conservative lower-bound estimate of cradle-to-gate impact. Energy consumption associated with bottle washing, shredding, and pelletisation was not directly measured and was therefore excluded from the base-case model. As these steps can be energy-intensive in industrial-scale mechanical recycling, their omission likely leads to a modest underestimation of the absolute GWP of rPET-based composites. However, because these pre-processing steps would apply equally to all three composite variants (UT, NT, and ST), the comparative conclusions regarding the marginal environmental impact of fibre surface treatment remain valid.

#### 4 Conclusions

The present investigation confirmed that surface modification of jute fibres significantly enhances the mechanical and structural performance of recycled PET composites. Experimental density increased from 1.22 g/cm<sup>3</sup> in the untreated (UT) composite to 1.24 g/cm<sup>3</sup> in the silane-treated (ST) composite, while porosity decreased from 3.9% to 2.4%, indicating improved consolidation and reduced internal void content. Mechanical performance improved consistently with fibre treatment. Tensile strength increased from 38.78 MPa (UT) to 48.29 MPa (ST), representing a 24.5% improvement over the untreated composite and a 50.5% increase relative to neat rPET (32.08 MPa). Flexural strength rose from 50.30 MPa (UT) to 68.84 MPa (ST), while short-beam shear strength increased from 11.74 MPa to 14.66 MPa. Hardness improved from 77 to 81 Shore D. One-way ANOVA confirmed statistically significant differences ( $p < 0.05$ ), with large effect sizes ( $\eta^2 = 0.79\text{--}0.96$ ). Porosity-based regression modelling produced  $R^2$  values of 0.631–0.916, with cross-validated  $R^2$  values of 0.391–0.861, confirming a strong inverse relationship between void content and mechanical response within the 2.4–3.9% porosity range. Life cycle assessment revealed low cradle-to-gate carbon footprints of 2.4912–2.5095 kg CO<sub>2</sub>-eq kg<sup>-1</sup>. It should be noted that these values represent a conservative lower bound of the actual cradle-to-gate impact, as energy inputs for bottle washing, shredding, and pelletising were excluded from the base-case model; inclusion of these energy-intensive recycling steps would increase the reported GWP. The silane treatment increased emissions by only 0.73% relative to UT, demonstrating that substantial mechanical gains were achieved with minimal environmental penalty. Overall, surface-engineered jute fibres provide a technically effective and environmentally viable route for upgrading recycled PET into higher-performance composite materials.

#### Supplementary Information

The online version contains supplementary material available at <https://doi.org/10.1007/s43939-026-00676-6>.

Supplementary Material 1

#### Author contributions

All authors contributed to the study's conception and design. Material preparation, data collection and analysis were performed by S.Saravana Mahesan, Senthil Babu, S.Thirumalai Kumaran, Oisik Das and Vigneshwaran Shanmugam. The first draft of the manuscript was written by G.Anbuhezhiyan and all authors provided language help, writing assistance and proof reading of the manuscript. All authors read and approved the final manuscript.

### Funding

Open access funding provided by Lulea University of Technology. This research did not receive any specific grant from funding agencies in the public, commercial, or not-for-profit sectors.

### Data availability

The data supporting the findings of this study, including the specimen-level experimental dataset and the Python scripts used for regression and life-cycle assessment (LCA), are provided in the Supplementary Materials.

### Declarations

#### Ethics approval and consent to participate

Not applicable.

#### Consent for publication

All authors consent to the publication of this work.

#### Competing interests

The authors declare no competing interests.

#### AI model transparency statement

ChatGPT (OpenAI, GPT-4o) was used for language editing and refinement. The authors are fully responsible for the content and interpretation of the manuscript. Spyder (Python IDE) was used to develop and execute the regression and life-cycle assessment (LCA) scripts employed in the data analysis.

Received: 21 November 2025 / Accepted: 23 April 2026

Published online: 14 May 2026

### References

1. Deeney M, Yates J, Banner J, Kadiyala S. Ending pollution and health harms from plastics. *BMJ*. 2025;388. <https://doi.org/10.1136/BMJ.R71>.
2. Global Waste Management Outlook 2024 | UNEP - UN Environment Programme. (n.d.). <https://www.unep.org/resources/global-waste-management-outlook-2024> (accessed November 13, 2025).
3. Bezeraj E, Debrie S, Arraez FJ, Reyes P, Van Steenberghe PHM, D'hooge DR, Edeleva M. State-of-the-art of industrial PET mechanical recycling: technologies, impact of contamination and guidelines for decision-making. *RSC Sustain*. 2025;3:1996–2047. <https://doi.org/10.1039/D4SU00571F>.
4. Ohnmacht H, Fiorillo C, Trossaert L, Reyes P, Cardon L, Edeleva M, D'hooge DR. Evaluating the Impact of Molecular Degradation on PETG Material Performance after Multiple Injection Molding Reprocessing Steps. *ACS Appl Polym Mater*. 2025;7:7942–57. <https://doi.org/10.1021/ACSAPM.5C00569>.
5. THE 17 GOALS | Sustainable Development. (n.d.). <https://sdgs.un.org/goals> (accessed November 13, 2025).
6. Chaudhary V, Ahmad F. A review on plant fiber reinforced thermoset polymers for structural and frictional composites. *Polym Test*. 2020;91:106792. <https://doi.org/10.1016/J.POLYMERTESTING.2020.106792>.
7. Djafari SR, Petroudy. Physical and mechanical properties of natural fibers, Advanced High Strength Natural Fibre Composites in Construction (2017) 59–83. <https://doi.org/10.1016/B978-0-08-100411-1.00003-0>
8. Techawinyutham L, Ayyappan V, Kumar M, Raghunathan V, Rangappa SM, Siengchin S. Sustainable epoxy composites from hemp/pineapple/glass fibers for lightweight automobile panels. *Int J Biol Macromol*. 2026;337:149392. <https://doi.org/10.1016/J.IJBIOMAC.2025.149392>.
9. Shahinur S, Alamgir Sayeed MM, Hasan M, Sayem ASM, Haider J, Ura S. Current Development and Future Perspective on Natural Jute Fibers and Their Biocomposites, *Polymers* 2022, Vol. 14, Page 1445 14 (2022) 1445. <https://doi.org/10.3390/POLYM14071445>
10. Biswas S, Ahsan Q, Cenna A, Hasan M, Hassan A. Physical and mechanical properties of jute, bamboo and coir natural fiber, *Fibers and Polymers* 2013 14:10 14 (2013) 1762–7. <https://doi.org/10.1007/S12221-013-1762-3>
11. Shahinur S, Hasan M, Ahsan Q, Saha DK, Islam MS. Characterization on the Properties of Jute Fiber at Different Portions. *Int J Polym Sci*. 2015;2015:262348. <https://doi.org/10.1155/2015/262348>.
12. Wang Wming, sheng Cai Z, yong Yu J, Xia Z. Changes in composition, structure, and properties of jute fibers after chemical treatments, *Fibers and Polymers* 2009 10:6 10 (2010) 776–780. <https://doi.org/10.1007/S12221-009-0776-3>
13. Komuraiah A, Kumar NS, Prasad BD. Chemical Composition of Natural Fibers and its Influence on their Mechanical Properties. *Mech Compos Mater* 2014. 2014;50:3. <https://doi.org/10.1007/S11029-014-9422-2>.
14. Chen CH, Chen CY, Lo YW, Mao CF, Liao WT. Characterization of alkali-treated jute fibers for physical and mechanical properties. *J Appl Polym Sci*. 2001;80:1013–20. <https://doi.org/10.1002/APP.1184;PAGEGROUP:STRING:PUBLICATION>.
15. Xie Y, Hill CAS, Xiao Z, Militz H, Mai C. Silane coupling agents used for natural fiber/polymer composites: A review. *Compos Part Appl Sci Manuf*. 2010;41:806–19. <https://doi.org/10.1016/J.COMPOSITESA.2010.03.005>.
16. Koohestani B, Darban AK, Mokhtari P, Yilmaz E, Darezereshki E. Comparison of different natural fiber treatments: a literature review. *Int J Environ Sci Technol* 2018. 2018;16:1. <https://doi.org/10.1007/S13762-018-1890-9>.
17. Hai NM, Kim BS, Lee S. Effect of NaOH treatments on jute and coir fiber PP composites. *Adv Compos Mater*. 2009;18:197–208. <https://doi.org/10.1163/156855109X428754>. ;WGROU:STRING:PUBLICATION.
18. Ravindran S, Sozhamannan GG, Venkatchalapathy VSK. Mechanical and water absorption behaviour on silane treated jute fiber based natural composites. *Mater Today Proc*. 2022;68:2134–41. <https://doi.org/10.1016/J.MATPR.2022.08.398>.
19. Arora G, Sharma H, Bhowmik P, Singh MK, Ayyappan V, Rangappa SM, Siengchin S. Recent Studies on Multiscale Modeling of Natural Fiber-Reinforced Composites. *Arch Comput Methods Eng*. 2025;2025:1–29. <https://doi.org/10.1007/S11831-025-10454-X>.

20. Sharma H, Arora G, Bhowmik P, Singh MK, Ayyappan V, Sehgal AK, Rangappa SM, Siengchin S. Predictive modeling of thermoplastic nanocomposites using machine learning algorithms. *Discover Mech Eng* 2025. 2025;4(4):1. <https://doi.org/10.1007/S44245-025-00134-2>.
21. Montgomery D, Peck CE, Vining AGG. *Introducing To Linear Regression Analysis* (5th ed.), John Wiley and Sons (2021) 642. <https://www.wiley.com/en-us/Introduction+to+Linear+Regression+Analysis%2C+6th+Edition-p-9781119578727> (accessed November 13, 2025).
22. M.C.D.& A.-C.C.C. Myers H Raymond, *Response Surface Methodology: Process and Product Optimization Using ...* Wiley Series in Probability And Statistics, 4th Ed., John Wiley& Sons Inc., New Jersey (2016) 894. <https://www.wiley.com/e-n-hk/Response+Surface+Methodology%3A+Process+and+Product+Optimization+Using+Designed+Experiments%2C+4th+Edition-p-9781118916018>(accessed November 13, 2025).
23. Mwesigwa R, Mwasiagi JI. Use of regression models to study the factors affecting the tensile and compressive properties of banana bio-composites. *J Nat Fibers*. 2019;16:1055–63. <https://doi.org/10.1080/15440478.2018.1448320>.
24. Taghipoor H, Mirzaei J. Statistical predicting and optimization of the tensile properties of natural fiber bio-composites. *Polym Bull* 2023. 2023;80(80):12. <https://doi.org/10.1007/s00289-023-04713-9>.
25. Mansor MR, Salit MS, Zainudin ES, Aziz NA, Ariff H. Life Cycle Assessment of Natural Fiber Polymer Composites. *Agricultural Biomass Based Potential Mater*. 2015;121–41. [https://doi.org/10.1007/978-3-319-13847-3\\_6](https://doi.org/10.1007/978-3-319-13847-3_6).
26. Korol J, Hejna A, Burchart-Korol D, Wachowicz J. Comparative Analysis of Carbon, Ecological, and Water Footprints of Polypropylene-Based Composites Filled with Cotton, Jute and Kenaf Fibers, *Materials* 2020, Vol. 13, Page 3541 13 (2020) 3541. <https://doi.org/10.3390/MA13163541>
27. Arya M, Skrifvars M, Khalili P. Performance and Life Cycle Assessment of Composites Reinforced with Natural Fibers and End-of-Life Textiles. *J Compos Sci* 2024. 2024;8:196. <https://doi.org/10.3390/JCS8060196>.
28. Nopparat N, Kianian B. Resource Consumption of Additive Manufacturing Technology. *Blekinge Institute of Technology*; 2012.
29. Tangram Technology Ltd, *Energy and Sustainability Topics-Energy management in plastics processing: A measurement framework*, n.d. [www.tangram.co.uk](http://www.tangram.co.uk). (accessed November 13, 2025).
30. Matarrese P, Fontana A, Sorlini M, Diviani L, Specht I, Maggi A. Estimating energy consumption of injection moulding for environmental-driven mould design. *J Clean Prod*. 2017;168:1505–12. <https://doi.org/10.1016/J.JCLEPRO.2017.07.144>.
31. Excellent CO2 balance | PET Recycling Team - A Member of the ALPLA Group. (n.d.). <https://petrecyclingteam.com/en/excellent-co2-balance> (accessed March 6, 2026).
32. Ostrowski KA, Romańska P, Spyrowski M. Material properties of recycled PET composites for structural anchoring and other civil engineering applications, *Scientific Reports* 2025 15:1 15 (2025) 36550-. <https://doi.org/10.1038/s41598-025-19291-1>
33. Bhawan S, Puram RK. CO 2 Baseline Database for the Indian Power Sector User Guide Government of India Ministry. of Power Central Electricity Authority; 2025.
34. Ramamoorthy SK, Bakare F, Herrmann R, Skrifvars M. Performance of biocomposites from surface modified regenerated cellulose fibers and lactic acid thermoset bioresin, *Cellulose* 2015 22:4 22 (2015) 2507–28. <https://doi.org/10.1007/S10570-015-0643-X>
35. Kassa LK, Jiru MG, Sinha DK, Gautam SS, Kumar A, Chauhan AK. Effect of NaOH Concentration, Fiber Length, Fiber Loading, and Filler Loading on the Mechanical Properties of Banana Fiber-Reinforced Polyester Composites. *Adv Mater Sci Eng*. 2025;2025:7707280. <https://doi.org/10.1155/AMSE/7707280>.
36. Karthikeyan A, Balamurugan K, Kalpana A. The effect of sodium hydroxide treatment and fiber length on the tensile property of coir fiber-reinforced epoxy composites. *Sci Eng Compos Mater*. 2014;21:315–21. <https://doi.org/10.1515/SECM-2013-0130/XML>.
37. Hong CK, Hwang I, Kim N, Park DH, Hwang BS, Nah C. Mechanical properties of silanized jute–polypropylene composites. *J Ind Eng Chem*. 2008;14:71–6. <https://doi.org/10.1016/J.JIEC.2007.07.002>.
38. Rajeshkumar G, Vignesh V, Mohan AMA, Prasaadh SVN, Poovarasan A, Ammarullah MI. Performance Analysis of NaOH-Treated Randomly Oriented Bauhinia Purpurea L Fiber/Epoxy (BPFE) Composites: Mechanical and Free Vibration Studies for Biomedical Applications. *J Nat Fibers*. 2025;22. <https://doi.org/10.1080/15440478.2025.2543119>.

## Publisher's note

Springer Nature remains neutral with regard to jurisdictional claims in published maps and institutional affiliations.